EXPERIMENTAL AND THEORETICAL INVESTIGATION OF VOLTAGE TRANSIENTS OF MAGNESIUM/MANGANESE DIOXIDE DRY CELLS IN ABSENCE OF ANODE-FILM BREAKDOWN

S. R. NARAYANAN and S. SATHYANARAYANA*

Department of Inorganic and Physical Chemistry, Indian Institute of Science, Bangalore 560 012 (India)

(Received March 18, 1988)

Summary

The film-covered anode/solution interface plays a crucial role in determining the performance of high-energy primary batteries based on lithium, magnesium, aluminium, etc. The present study describes improvements over earlier attempts to analyze voltage transients of magnesium/manganese dioxide (Mg/MnO_2) dry cells for the non-destructive evaluation of the electrochemical properties of the film-covered magnesium/solution interface. Equivalent-circuit analogs for the anode/solution interface are proposed and the most plausible set of models identified. The anode-film resistance and its temperature dependence are evaluated. The technique developed for Mg/MnO_2 cells can be extended, in principle, to other battery systems based on lithium, aluminium, calcium, etc., and can be exploited for quality control and design optimization of such cells.

Introduction

Primary batteries based on lithium and magnesium are characterized by high specific energy and long shelf life. The latter property is due to the presence of a protective film on the surface of the reactive metal anode. The passive film is either spontaneously formed on contact with battery electrolyte or is applied as a coating during manufacture [1 - 3]. Inadequate passivation results in failure of the cell by anode corrosion, while excessive passivation causes a long delay in the attainment of the operating voltage following discharge of the cell [3, 4]. Since the film-covered anode exerts such a strong influence on battery performance [5], it is important to evaluate the interfacial electrochemical properties of the film.

Although good protection of the reactive metal anode is achieved during storage, the film breaks down at the slightest attempt to discharge the cell [1]. Therefore, the method employed to investigate the properties

*Author to whom correspondence should be addressed.

0378-7753/88/$3.50

of the film-covered anode/solution interface must not cause breakdown of the passive film. In an earlier study [5], a non-destructive electrochemical technique was proposed to evaluate the anode-film resistance and the capacity of magnesium/manganese dioxide (Mg/MnO_2) dry cells. In brief, the method is based on the measurement and interpretation of voltage transients that are obtained when the cells are discharged galvanostatically. The current density is kept small (*i.e.*, $10^{-8} - 10^{-9}$ A cm^{-2}) so that the delicate passive film on the magnesium anode is not damaged. Experimental criteria were established to demonstrate the intactness of the protective passive film during the test. A theoretical interpretation of the cell voltage transients, observed during both discharge and subsequent open-circuit, leads to the evaluation of the film properties. Being non-destructive in character, the technique overcomes the limitations of earlier attempts [6, 7] to evaluate the electrochemical properties of the film-covered anode/solution interface.

The non-destructive technique described above is open to further improvement. Possible approaches to achieving such an improvement include the following.

(i) Determination of the electrical equivalent-circuit model that best describes the physical situation at the film-covered anode/solution interface. Note, the previous theoretical analysis considers only one electrical equivalent-circuit model to interpret the cell voltage transient. However, several other electrical equivalent-circuits *per se* consistent with the phenomenological description of the film-covered anode/solution interface [8], may be analyzed to identify the equivalent-circuit model that best describes the physical situation.

(ii) Provision in the theoretical analysis for a double-layer capacitance at the metal/film interface in order to identify its contribution to the measured capacitance.

(iii) Reduction of the drop in steady-state cell voltage during the test discharge to less than 5 mV in order to validate to a greater extent the assumptions made in the theoretical analysis.

(iv) Decrease in the discharge current density to reduce further the test perturbations.

In the present study, new experimental data have been obtained for cell voltage transients of Mg/MnO_2 dry cells when discharged galvanostatically at $10^{-10} - 10^{-11}$ A cm^{-2} (anode current density). Experiments were carried out at 0 °C and 23 °C to investigate the dependence of film properties on temperature and its correlation with the observed dependence of delay time on temperature [9]. Diagnostic criteria derived from the theoretical analysis of four plausible electrical equivalent circuits have been applied to the experimental results in order to deduce the model(s) that best describe(s) the physical situation prevailing at the film-covered anode/solution interface. The experimental technique and method of analysis, although demonstrated with the Mg/MnO_2 dry cell can, in principle, be extended to study the film properties in cells employing other reactive metal anodes such as lithium and aluminium.

Experimental

Test cells

All experiments were conducted with CD-size, cylindrical Mg/MnO_2 dry cells manufactured by Messrs. Bharat Electronics Ltd., India. These cells had a nominal capacity of 2.5 A h at 25 °C when discharged at 500 mA. The magnesium anode had a proprietary passivation coating of fatty acid esters and chromate.

Electrical circuit for discharge under galvanostatic conditions without causing anode-film breakdown

In order to discharge the Mg/MnO_2 cell galvanostatically at extremely low rates (10^{-10} - 10^{-11} A cm^{-2}, anode current density) and to record the cell voltage transient, the specially designed electrical circuit described earlier [5] was used with the modifications shown in Fig. 1. The sequence of operations in a typical experiment was as follows.

Using an electrometric amplifier/digital voltmeter combination, the open-circuit cell voltage was measured to ±0.1 mV. The potential difference between A and A′ was set to drive the desired discharge current through the test cell and R_3 by closure of switch S. The cell voltage was then backed off to ~1 mV using B_2 and R_2 with switch S closed to record the cell voltage transient. The discharge current was calculated from the voltage drop across R_3; the latter was measured with an electrometric voltmeter. When a steady-state cell voltage was reached, the switch S was opened and the open-circuit cell voltage recovery transient recorded until the open-circuit value again became constant. For each cell, the cell voltage transients were recorded

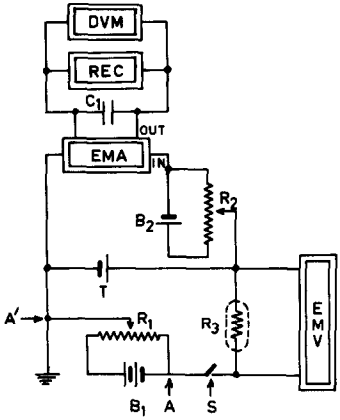

Fig. 1. Electrical circuit for the discharge of Mg/MnO_2 dry cells at constant current without anode-film breakdown. T = test cell; R_1, R_2 = 50 kΩ, ten-turn helical potentiometers; R_3 = 10 MΩ high stability, shielded, current limiting resistor; B_1 = nickel/cadmium cells (at 50% state-of-charge); B_2 = Li/SO_2 cell (D-size, Duracell); EMA = electrometric amplifier (Wenking PPT 75); REC = recorder (Rikadenki WE 201); EMV = electrometric voltmeter (Philips PP 9046); C_1 = 10 μF low-loss polystyrene capacitor; DVM = digital voltmeter (HIL 2301).

for five successive values of discharge current in the range 1 - 12 nA, starting from the lowest value. Experiments were carried out at 0 °C and 23 °C, and repeated with seven cells to obtain a reliable average.

The following special features of the electrical circuit were required in order to attain the unusually high sensitivity in voltage measurement.

(i) As the test currents were 1 - 12 nA, the voltage measurement employed electrometric amplifiers with high input impedance ($>10^{13}$ Ω) to keep the sensing currents for voltage measurement well below the test currents employed.

(ii) Under the test conditions, the drop in the cell voltage in the steady-state was 1 - 3 mV, and the voltage transient was recorded at a sensitivity of ±5 μV. Thus, a stable voltage back-off employing an Li/SO_2 cell (B_2 in Fig. 1) with a typical drift of 10 μV h^{-1} was necessary to attain the high sensitivity of voltage measurement.

(iii) The environmental temperature was controlled to ±0.5 °C to minimise voltage variations arising from dissimilar metal-junction and cell potential differences which otherwise could affect the sensitivity of the voltage measurement.

(iv) The discharge current was measured as a voltage drop across the precision resistor R_3. This was achieved with a high input impedance electrometer that was energised by a 9 V floating battery supply, rather than by a.c. mains supply, in order to avoid earth loops.

(v) Teflon-coated wires were used for inter-connection of the components to minimise leakage currents. All high-impedance elements were shielded and the shields grounded. A low-loss, 10 μF capacitor, connected across the input of the recorder, was used to shunt disturbances from line transients. In this manner, noise pick-up was minimised. To ensure protection from moisture, the basic electrical circuit was enclosed in an acrylic box containing absorbent silica gel.

Constant-resistance discharge without anode-film breakdown

Discharge experiments similar to those described above may be carried out across a constant resistance, ensuring that the discharge current does not exceed 10^{-7} A for a CD-size Mg/MnO_2 dry cell. In the former case, the discharge current is not constant with time. In the present study, however, the maximum variation in cell voltage is just 1% of the total cell voltage, and consequently no significant change in the discharge current is to be expected. Since discharge across a constant resistance without anode-film breakdown must employ resistances of the value of 10^3 - 10^5 MΩ, it is necessary to maintain stricter control of the environmental conditions in order to avoid changes in the values of these resistances. For these reasons, constant-current discharge was preferred to discharge across a constant load resistance.

Discharge of Mg/MnO_2 dry cells leading to anode-film breakdown

The cells subjected to the non-destructive constant-current discharge experiments were discharged at constant current in the range 0.01 - 10 mA

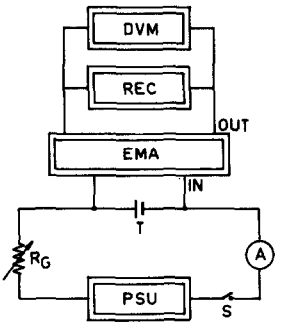

Fig. 2. Electrical circuit for the discharge of Mg/MnO_2 dry cells at constant current (0.01 - 10 mA, accompanied by anode-film breakdown) and observation of cell voltage transient.

during which the anode-film suffers breakdown. The cell voltage transients were recorded employing the galvanostatic discharge circuit shown in Fig. 2 for several values of constant discharge current in a specified range. These experiments, as will be shown later, are required to obtain the internal resistance of the cell under conditions when the anode is film-free.

Results

The cell voltage transients observed during discharge at constant current without causing anode-film breakdown at 0 °C and 23 °C are shown in Figs. 3 and 4. These transients follow a markedly different course from those observed during the initial moments of discharge at currents in the range 0.1 - 0.5 A (Fig. 5) which cause anode-film breakdown. In particular, both the characteristic voltage dip on initiation of discharge and the voltage

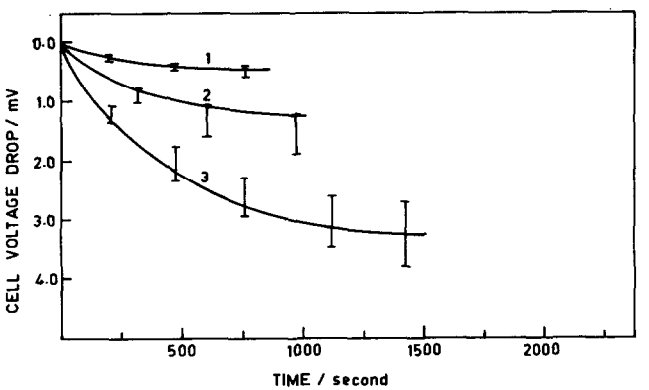

Fig. 3. Galvanostatic discharge transients at 0 °C for Mg/MnO_2 dry cells (nominal capacity = 2.5 A h; anode area = 100 cm^2). Discharge current: (1) 1.0; (2) 3.0; (3) 5.0 nA. Range of values are for five cells tested at each current.

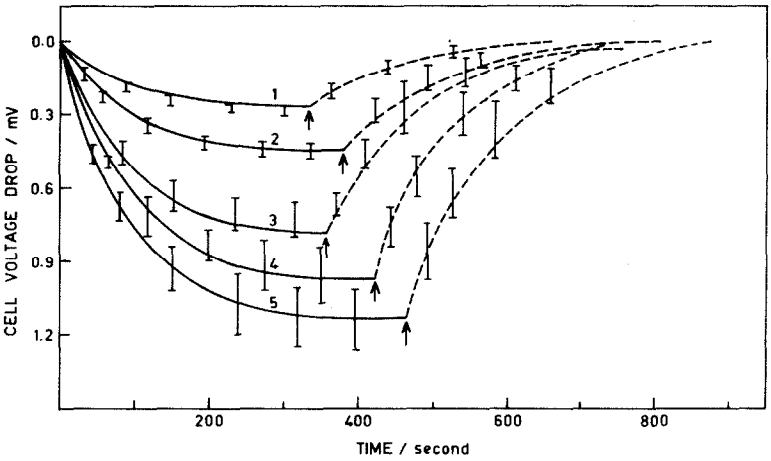

Fig. 4. Galvanostatic discharge and subsequent open-circuit recovery transients at 23 °C for typical Mg/MnO_2 dry cells (nominal capacity 2.5 A h; anode area: 100 cm^2). Discharge currents: (1) 3.0; (2) 5.0; (3) 8.0; (4) 10.0; (5) 12.0 nA. Arrow indicates start of open-circuit voltage measurements. Range of values is for seven cells tested at each current.

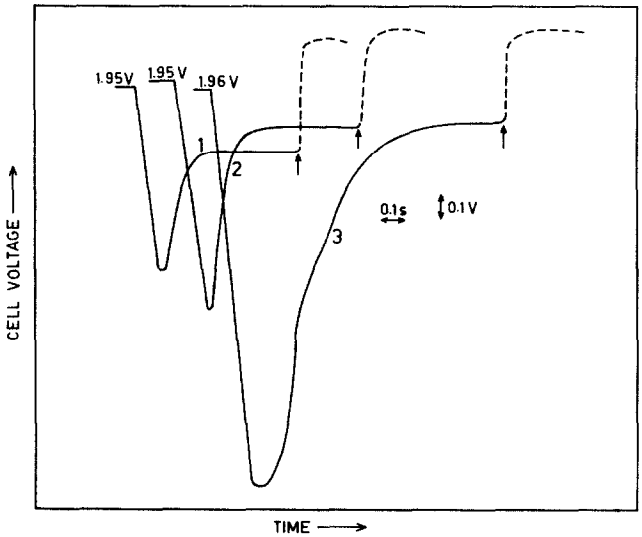

Fig. 5. Galvanostatic discharge and subsequent open-circuit transients at 23 °C for Mg/MnO_2 dry cells (nominal capacity: 2.5 A h; anode area = 100 cm^2). Discharge currents: (1) 0.5; (2) 0.2; (3) 0.1 A. Arrow indicates start of open-circuit voltage measurements.

overshoot on termination of discharge, observed in Fig. 5, are absent in Figs. 3 and 4. Also, the magnitude of the steady-state cell-voltage drop at 0 °C is about six times larger than that at 23 °C for discharge currents of 10^{-8} - 10^{-9} A (*cf.* Fig. 3 and Fig. 4).

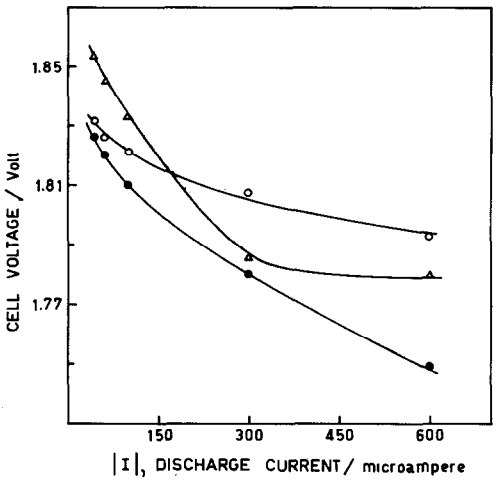

Fig. 6. Steady-state galvanostatic polarisation curves at 23 °C for three Mg/MnO_2 dry cells (1 - 3) at discharge currents in range 35 - 60 μA.

The steady-state cell voltage attained on discharge at constant current in the range 0.01 - 10 mA (during which anode-film breakdown occurs) is plotted in Figs. 6 and 7.

The "delay" time for the attainment of a particular operating cell voltage under practical conditions of discharge at 0 °C and 23 °C is shown in Table 1.

In the following sections, the above experimental results are interpreted to obtain information on the physicochemical processes at the film-covered anode/solution interface in Mg/MnO_2 dry cells.

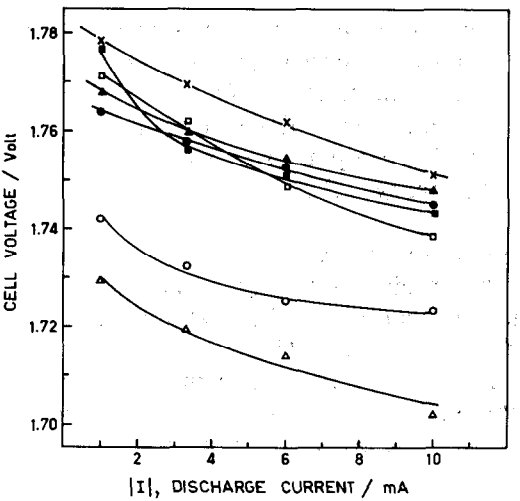

Fig. 7. Steady-state galvanostatic polarisation curves at 23 °C for seven Mg/MnO_2 dry cells (1 - 7) at discharge currents 1 - 10 mA.

TABLE 1

Time for Mg/MnO_2 cells at 0 °C and 23 °C to reach a voltage of 1.35 V during discharge across 4 Ω

Cell batch	Time (s)	
	0 °C	23 °C
1	2.62	0.78
	2.22	0.78
	2.06	0.80
2	2.23	0.70
	1.96	0.76
	2.14	0.76
3	2.52	0.80
	2.80	0.84
	2.10	0.62

Theoretical aspects

Several criteria have been established [5] to demonstrate the absence of anode-film breakdown in Mg/MnO_2 dry cells when discharged at 10^{-10} - 10^{-11} A cm^{-2} (anode current density). In summary, these are as follows:

(i) the quantity of anodic product resulting from a typical test discharge corresponds to 0.015% of a monolayer of $Mg(OH)_2$;

(ii) the characteristic voltage dip on initiation of discharge (corresponding to anode-film breakdown), and the voltage overshoot (corresponding to anode repassivation) observed at practical rates of discharge, are both absent at ultra-low rates;

(iii) the cell voltage transients can be reproduced quantitatively by repeating the experiments with the same cell, indicating thereby that the test does not cause any change in the state-of-passivation of the anode.

By virtue of the above criteria, the transient voltage response may be used reliably to evaluate the electrochemical properties of the film-covered anode/solution interface in high-energy primary cells.

Physical model of film-covered anode/solution interface

Under the conditions of the test experiment during which the anode-film remains intact, the electrochemical response of the Mg/MnO_2 dry cell is governed by the physical model shown in Fig. 8. The magnesium anode, covered by a thin dielectric passive film of inhibitors*, is in contact with the electrolyte solution. The magnesium/film interface sustains the anodic dissolution reaction and is associated with a polarisation resistance and a

*The actual composition of the film may be quite complex and is not crucial to the model.

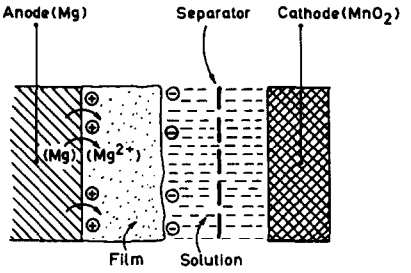

Fig. 8. Physical model of Mg/MnO_2 dry cell without anodic-film breakdown.

double layer capacitance. (This aspect was ignored in the earlier study [5].) The passive film presents a resistance as well as a capacitance. Diffusion of reactants and products occurs at the metal/film interface and through the bulk of the film. The solution, the separator, and the constituents of the cathode mix give rise to an ohmic resistance. Since the MnO_2 cathode is a large-area porous electrode of low polarisability, its impedance is negligible in comparison with that of the smooth, concentric Mg anode.

Electrical equivalent circuits

Four plausible electrical equivalent circuits consistent with the above phenomenological description of the Mg/MnO_2 dry cell with anode-film intact are shown in Fig. 9. These include: the charge-transfer resistance, R_1, associated with a double-layer capacitance, C_1; the capacitance of the film C_2; film resistance R_2; the ohmic resistance, R_d, of the solution, the

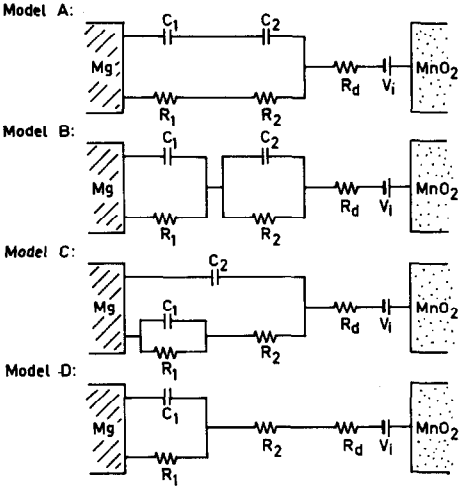

Fig. 9. Electrical equivalent-circuit models for Mg/MnO_2 dry cell with anode-film intact under conditions when diffusional impedance is negligible. R_1: charge-transfer resistance; R_2: film resistance; R_d: resistance of electrolyte and separator; C_1: double-layer capacitance; C_2: film capacitance; V_i: open-circuit voltage of cell.

separator, and the cathode mix. The diffusion impedance of reactants and products may be neglected for the reasons discussed in detail elsewhere [8] and briefly presented in the following:

(i) since the test currents are of the order of 10^{-10} A cm^{-2}, the concentration gradients arising from the test perturbations are too small to include accumulation/depletion effects;

(ii) since the characteristic time required for equalization of the concentration differences across the passive film (thickness: 10 - 100 Å), assuming a diffusion coefficient of $\sim 10^{-5}$ cm^2 s^{-1}, is 10^{-7} s, the gradients, even if set up, would vanish in so short a time as not to be reflected in the course of an experiment lasting about 1000 s.

The equivalent circuits of Fig. 9 may now be analysed to obtain the theoretical cell voltage response during discharge at ultra-low rates.

Analysis of cell voltage transients in absence of anode-film breakdown

In the theoretical analysis of cell voltage transients during discharge with anode-film intact, three cases may be considered:

(i) analysis of cell voltage transient on initiating discharge at constant current;

(ii) analysis of cell voltage transient on initiating discharge across a constant resistance;

(iii) analysis of open-circuit recovery transient following termination of discharge by constant current and by constant resistance modes.

In accordance with the physical model proposed above and with the experimental conditions of discharge (*viz.*, 10^{-10} - 10^{-11} A; maximum voltage drop 3 mV; discharge time 5 s), the following general assumptions may be made:

General assumptions and relationships

(i) Mass-transfer polarisation is absent;

(ii) R_1, R_2, R_d, C_1 and C_2 are independent of potential and time;

(iii) impedance of the MnO_2 cathode is negligible.

The open-circuit voltage of the cell V_i, is given by:

$$V_i = (E_c - E_a)_{I=0} \tag{1}$$

where E_c is the single electrode potential of the MnO_2 cathode and E_a is that of the magnesium anode. Under open-circuit conditions, the potential of the magnesium anode is a mixed potential governed by the magnesium ionisation reaction and the conjugate cathodic reaction of hydrogen evolution. Thus, E_a may be replaced under open-circuit conditions by E_{cor} representing the corrosion potential of the Mg anode. Equation (1) therefore becomes:

$$V_i = E_c - E_{cor} \tag{2}$$

During discharge at a constant current $|I|$ where I is the current through the anode*, the cell voltage V may be expressed as

$$V = E_c - E + IR_d \tag{3}$$

where E is the observable single electrode potential of the magnesium anode during discharge, *i.e.*, the potential that would be observed if measured with a reference electrode; R_d is the ohmic resistance of the electrolyte, the separator, and the cathode mix. All other polarisation effects are included in the observable single electrode potential, E. Polarisation effects at the cathode being negligible, eqns. (2) and (3) give

$$E - E_{cor} = V_i - V + IR_d \tag{4}$$

During discharge across a constant resistance, R_L, the discharge current I is dependent on the cell voltage V as follows:

$$I = -\frac{V}{R_L} \tag{5}$$

From eqns. (3) and (5):

$$V = \frac{R_L(E_c - E)}{R_L + R_d} \tag{6}$$

From eqns. (3) - (6)

$$E - E_{cor} = V_i - \left(\frac{R_L + R_d}{R_L}\right) V \tag{7}$$

On termination of discharge an open-circuit condition is effected and the discharge current, I, is zero. Thus, in the open-circuit condition, represented by an asterisk (*), the cell voltage is related to the single electrode potentials of the magnesium anode (E^*) and the MnO_2 cathode (E_c) by:

$$E^* - E_c = V^* \tag{8}$$

From eqns. (2) and (8)

$$E^* - E_{cor} = V_i - V^* \tag{9}$$

Cell voltage transient

With these general assumptions and relationships, the following three types of cell voltage transient may be considered separately.

Cell voltage transient under constant-current discharge. Figure 10(a) shows four equivalent circuit models (A - D) that represent the Mg/MnO_2 dry cell under constant-current discharge with anode-film intact.

*Anodic current is taken as negative; single electrode potentials conform to the International convention.

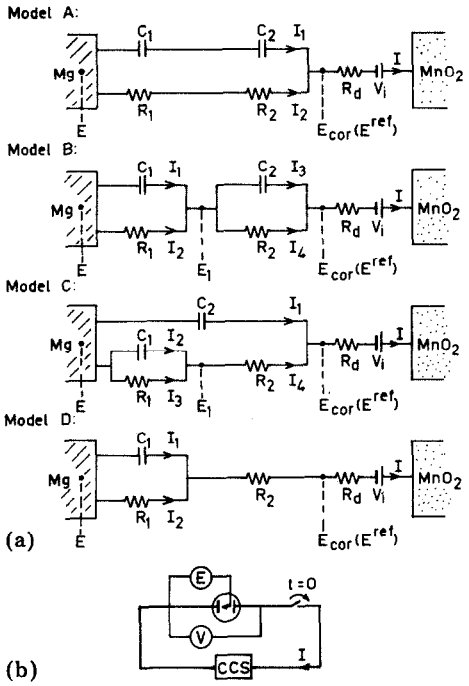

Fig. 10. (a) Electrical equivalent-circuit models A, B, C, and D representing Mg/MnO_2 dry cell during discharge at constant current, I, without anode-film breakdown; (b) schematic of electrical circuit used in test. CCS: constant-current supply; E: single electrode potential of Mg anode. For convenience, reference electrode potential (E^{ref}) taken as steady-state corrosion potential (E_{cor}) of anode. Note: Anodic current, I, is negative; arrows indicate direction of conventional electric current.

The schematic electric circuit given in Fig. 10(b) indicates that on closure of the switch, a constant current, I, flows through the cell.

The discharge current, I, may be expressed in terms of the branch currents I_1, I_2, I_3, and I_4 for each of the models according to Kirchoff's law. The observable single electrode potential of the anode, E, may then be expressed in terms of the branch currents. Since the total cell voltage drop during the test experiment is about 3 mV or less (see Figs. 3, 4), the overpotential at the anode ($E - E_{cor}$) is small compared with $RT/\alpha nF$ or $RT/\beta nF$, where α and β are the transfer coefficients for the cathodic and anodic conjugate reactions of corrosion. Thus, a linear polarisation regime may be assumed to prevail during the experiment for the charge-transfer process at the Mg anode.

The differential equation relating ($E - E_{cor}$) and I may now be set up and solved, the integration constants being evaluated with suitable boundary conditions. Finally, ($E - E_{cor}$) may be transformed in terms of the cell voltage through eqn. (4), leading to the theoretical description of the cell voltage transient. Such an analysis has been presented in detail for the

TABLE 2

Theoretical cell voltage transient under constant-current discharge of Mg/MnO_2 dry cell *without* anode-film breakdown

Model (Fig. 10(a))	Theoretical voltage transient	Boundary conditions
A	$V = V_i + I\left[(R_1 + R_2 + R_d) - (R_1 + R_2)\exp\left\{-\frac{(C_1 + C_2)}{(R_1 + R_2)C_1C_2}\,t\right\}\right]$	$t = 0^+$, $V_{(t=0^+)} = V_i + IR_d$
B	$V = V_i + I\left[(R_1 + R_2 + R_d) - R_1\exp\left(-\frac{t}{R_1C_1}\right) - R_2\exp\left(-\frac{t}{R_2C_2}\right)\right]$	$t = 0^+$, $E = E_i = E_{cor}$ (see Fig. 10(a))
C	$V = V_i + I(R_1 + R_2 + R_d) + \frac{1}{b}\{K_1\exp(-r_1t) + K_2\exp(-r_2t)\}$	$t = 0^+$, $V_{(t=0^+)} = V_i + IR_d$
	K_1, K_2, r_1, r_2 and b are as defined in Appendix 1	
D	$V = V_i + I\left[(R_1 + R_2 + R_d) - R_1\exp\left(-\frac{t}{R_1C_1}\right)\right]$	$t = 0^+$, $V_{(t=0^+)} = V_i + I(R_2 + R_d)$

relatively complex case of Model C in Appendix 1. Results for the other models are given in Table 2.

From Table 2, it can be seen that theory predicts that a steady-state discharge voltage will be reached in all the models. If V_∞ is the value of cell voltage at $t \to \infty$, then for all the models:

$$V_i - V_\infty = -I(R_1 + R_2 + R_d) \tag{10}$$

If $V_{(t=0^+)}$ is the instantaneous cell voltage on initiation of discharge, then for models A, B and C:

$$V_i - V_{(t=0^+)} = -IR_d \tag{11}$$

whereas for model D:

$$V_i - V_{(t=0^+)} = -I(R_2 + R_d) \tag{12}$$

Several other implications that follow from Table 2 are summarised in Table 3.

Cell voltage transient during discharge across constant resistance. The discharge across a constant resistance (load) is distinguished from the constant-current discharge (see above) in that the discharge current is no longer independent of time during the course of the transient. The load resistance may be so chosen that the average current during discharge is in the range in which anode-film breakdown does not occur. The physical situation prevailing under the conditions of discharge of the Mg/MnO_2 dry cell across a constant resistance (R_L) governed by the four models is shown in Fig. 11(a). The schematic electric circuit (Fig. 11(b)) shows that on closure of the switch, discharge across the constant resistance is initiated. The transient cell voltage response may now be obtained for all the models in a manner similar to that discussed above for constant-current discharge. The theoretical results are summarised in Table 4. The analysis for the relatively complex case of Model C is given in Appendix 2.

The results of Table 4 show that as $t \to \infty$, a steady-state cell voltage is approached given by $V_\infty = V_i R_L/R$, where $R = R_1 + R_2 + R_d + R_L$. Implications similar to the case of constant-current discharge (Table 3) may also be deduced but are not detailed here.

Open-circuit cell voltage transient following termination of discharge. Analysis of the two cell voltage discharge transients discussed above predicts the attainment of a steady-state, closed-circuit cell voltage during discharge. On termination of the discharge, an open-circuit condition is effected (shown schematically in Fig. 12(b)). The theoretical analysis of the open-circuit cell voltage recovery transient of the Mg/MnO_2 dry cell, governed by the four equivalent circuit models (shown in Fig. 12(a)) may be carried out for both constant-current and constant-resistance discharge. The analysis for Model C is presented in Appendix 3. The theoretical results are summarised in Tables 5 and 6. The latter indicate that as $t \to \infty$ a steady-state,

TABLE 3

Implications arising from theoretical results of cell voltage transients given in Table 2

Model	Conditions	Implications
A	For $t \ll \dfrac{(R_1 + R_2)C_1C_2}{(C_1 + C_2)}$	$V_i - V \approx -I\left\{R_d + \dfrac{C_1 + C_2}{C_1C_2}t\right\}$
B	(i) For $\dfrac{1}{R_1C_1} = \dfrac{1}{R_2C_2} = \dfrac{1}{RC}$	$V - V_\infty \approx -I(R_1 + R_2)\exp\left(-\dfrac{t}{RC}\right)$
	(ii) For $t \lesssim R_1C_1 \ll R_2C_2$	$V - V_\infty \approx -I\left\{R_1\exp\left(-\dfrac{t}{R_1C_1}\right) + R_2 - \dfrac{t}{C_2}\right\}$
	(iii) For $t \lesssim R_2C_2 \ll R_1C_1$	$V - V_\infty \approx -I\left\{R_2\exp\left(-\dfrac{t}{R_2C_2}\right) + R_1 - \dfrac{t}{C_1}\right\}$
	(iv) For $t \ll R_1C_1 \ll R_2C_2$	$V_i - V \approx -I\left\{R_d + \left(\dfrac{1}{C_1} + \dfrac{1}{C_2}\right)t\right\}$
	(v) For $R_2C_2 \gg R_1C_1$ and $t \gtrsim R_2C_2 \gg R_1C_1$	$V - V_\infty \approx -IR_2\exp\left(-\dfrac{t}{R_2C_2}\right)$
C	(i) $\dfrac{1}{r_1} \approx \dfrac{1}{r_2} \approx \dfrac{1}{r}$	$V - V_\infty = \dfrac{1}{b}(K_1 + K_2)\exp(-rt)$
	(ii) $t \lesssim \dfrac{1}{r_1} \ll \dfrac{1}{r_2}$	$V - V_\infty = \dfrac{1}{b}\{K_1\exp(-r_1t) + K_2(1 - r_2t)\}$
	(iii) $t \lesssim \dfrac{1}{r_2} \ll \dfrac{1}{r_1}$	$V - V_\infty = \dfrac{1}{b}\{K_2\exp(-r_2t) + K_1(1 - r_1t)\}$
	(iv) $t \ll \dfrac{1}{r_1} \ll \dfrac{1}{r_2}$	$V_i - V = -I\{R_d + (K_1r_1 + K_2r_2)t\}$
D	$t \ll R_1C_1$	$V_i - V = -I\left\{(R_2 + R_d) + \dfrac{t}{C_1}\right\}$

TABLE 4

Theoretical cell voltage transient during discharge of Mg/MnO_2 dry cell across a constant resistance *without* anode-film breakdown

Model (Fig. 11(a))	Theoretical cell voltage transient	Boundary conditions
A	$V = \frac{V_i R_L}{R_L + R_d}\left[1 - \frac{R_1 + R_2}{R}\left(1 - \exp\left\{1 - \frac{Rt}{(R_1 + R_2)(R_L + R_d)C}\right\}\right)\right]$ $R = R_1 + R_2 + R_L + R_d;\ C = C_1C_2/(C_1 + C_2)$	at $t = 0^+$, $V_{(t=0^+)} = \frac{V_i R_L}{(R_L + R_d)}$
B	$V = \frac{1}{b}\{K_1 \exp(-r_1 t) + K_2 \exp(-r_2 t) - c\}$*	at $t = 0^+$, $V_{(t=0^+)} = \frac{V_i R_L}{(R_L + R_d)}$
C	$V = \frac{1}{b}\{K_1 \exp(-r_1 t) + K_2 \exp(-r_2 t) - c\}$**	at $t = 0^+$, $V_{(t=0^+)} = \frac{V_i R_L}{(R_L + R_d)}$
D	$V = \frac{V_i R_L}{R}\left[1 + \frac{R_1}{R_2 + R_L + R_d} \exp\left\{-\frac{Rt}{R_1 C_1 (R_L + R_d)}\right\}\right]$	at $t = 0^+$, $V_{(t=0^+)} = \frac{V_i R_L}{(R_2 + R_L + R_d)}$

*$a = \frac{1}{R_1C_1} + \frac{1}{R_2C_2} + \frac{1}{(R_L + R_d)C}$; $b = \frac{R_1 + R_2 + R_L + R_d}{R_1C_1R_2C_2(R_L + R_d)}$; $c = \frac{V_i R_L}{R_1C_1R_2C_2(R_L + R_d)}$; $r_1, r_2 = \frac{a \pm (a^2 - 4b)^{1/2}}{2}$; K_1, K_2 integration constants.

**K_1, K_2, r_1, r_2, b and c as defined in Appendix 2.

TABLE 5

Theoretical description of open-circuit cell-voltage recovery transient following termination of constant-current discharge

Model (Fig. 10(a))	Theoretical description	Boundary conditions
A	$V^* = V_i + I(R_1 + R_2)\exp\left\{-\dfrac{t(C_1 + C_2)}{(R_1 + R_2)C_1C_2}\right\}$	at $t = 0^+$, $V^*_{(t=0^+)} = V_i + I(R_1 + R_2)$
B	$V^* = V_i + I\left\{R_1 \exp\left(-\dfrac{t}{R_1C_1}\right) + R_2 \exp\left(-\dfrac{t}{R_2C_2}\right)\right\}$	at $t = 0^+$, $V^*_{(t=0^+)} = V_i + I(R_1 + R_2)$
C	$V^* = \dfrac{1}{b}\{K_1 \exp(-r_1t) + K_2 \exp(-r_2t) - c\}$ $K_1, K_2, r_1, r_2, b,$ & c as defined in Appendix 3	at $t = 0^+$, $V^*_{(t=0^+)} = V_i + I(R_1 + R_2)$
D	$V^* = V_i + IR_1 \exp\left(-\dfrac{t}{R_1C_1}\right)$	at $t = 0^+$, $V^*_{(t=0^+)} = V_i + IR_d$

TABLE 6

Theoretical description of open-circuit voltage recovery transient following termination of discharge across a constant resistance without anode-film breakdown

Model (Fig. 12(a))	Theoretical description	Boundary conditions
A	$V_i - V^* = \frac{V_i(R_1 + R_2)}{R} \exp\left\{-\frac{(C_1 + C_2)t}{(R_1 + R_2)C_1C_2}\right\}$	at $t = 0^+$, $V^*_{(t=0^+)} = \frac{V_i(R_L + R_d)}{R}$
	$R = (R_1 + R_2 + R_d + R_L)$	where $R = R_1 + R_2 + R_L + R_d$
B	$V_i - V^* = \frac{V_i}{R}\left\{R_1 \exp\left(-\frac{t}{R_1C_1}\right) + R_2 \exp\left(-\frac{t}{R_2C_2}\right)\right\}$	at $t = 0^+$, $V^*_{(t=0^+)} = \frac{V_i(R_L + R_d)}{R}$
C	$V^* = \frac{1}{b}\{K_1 \exp(-r_1t) + K_2 \exp(-r_2t) - c\}$	at $t = 0^+$, $V^*_{(t=0^+)} = \frac{V_i(R_L + R_d)}{R}$
	K_1, K_2, r_1, r_2, b and c as defined in the Appendix	
D	$V_i - V^* = \frac{V_iR_1}{R} \exp\left(-\frac{t}{R_1C_1}\right)$	at $t = 0^+$, $V^*_{(t=0^+)} = \frac{V_i(R_L + R_2 + R_d)}{R}$

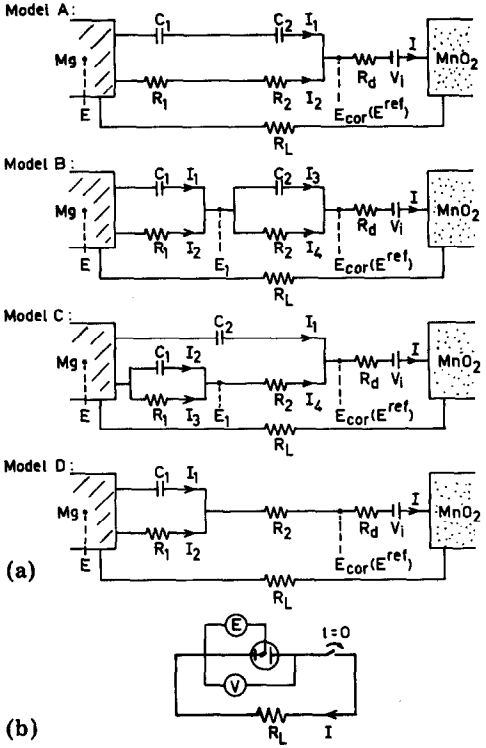

Fig. 11. (a) Electrical equivalent-circuit models A, B, C, and D representing Mg/MnO_2 dry cell during discharge across a constant resistance, R_L, without anode-film breakdown; (b) schematic of electrical-circuit used in test. R_L: constant-load resistance; E: the single electrode potential of the Mg anode. Conditions for E^{ref} and I as in Fig. 10.

open-circuit cell voltage is attained and is equal to V_i. Immediately following the termination of the constant-current discharge (the condition designated as $t = 0^+$), the cell voltage for models A, B and C is given by:

$$V^*_{(t=0^+)} = V_\infty - IR_d \tag{13}$$

while for model D:

$$V^*_{(t=0^+)} = V_\infty - I(R_2 + R_d) \tag{14}$$

The other implications arising out of the results of Table 5 are summarised in Table 7.

Comparison of experimental results with theory

Based on the results of theoretical analysis, several diagnostic criteria may be deduced to compare experimental results with theory. These criteria, summarised in Tables 8 and 9, may now be applied to the experimental

TABLE 7

Implications arising from the theoretical results of open-circuit cell voltage transients of Table 5

Model	Conditions	Implications
A	$t \ll \dfrac{(R_1 + R_2)C_1C_2}{C_1 + C_2}$	$V^* - V_\infty = -I\left\{R_d - \dfrac{C_1 + C_2}{C_1C_2}\,t\right\}$
B	(i) $R_1C_1 \approx R_2C_2 \approx RC$	$V_i - V^* = -I(R_1 + R_2)\exp\left(-\dfrac{t}{RC}\right)$
	(ii) For $t \lesssim R_1C_1 \ll R_2C_2$	$V_i - V^* = -I\left\{R_1\exp\left(-\dfrac{t}{R_1C_1}\right) + R_2 - \dfrac{t}{C_2}\right\}$
	(iii) For $t \lesssim R_2C_2 \ll R_1C_1$	$V_i - V^* = -I\left\{R_2\exp\left(-\dfrac{t}{R_2C_2}\right) + R_1 - \dfrac{t}{C_1}\right\}$
	(iv) For $t \ll R_1C_1 \ll R_2C_2$	$V^* - V_\infty = -I\left\{R_d + \left(\dfrac{1}{C_1} + \dfrac{1}{C_2}\right)t\right\}$
	(v) For $t \gtrsim R_2C_2 \gg R_1C_1$ $t \gtrsim R_1C_1 \gg R_2C_2$ is unrealistic as $R_2 \gg R_1$	$V_i - V^* = -IR_2\exp\left(-\dfrac{t}{R_2C_2}\right)$
C	(i) $\dfrac{1}{r_1} \approx \dfrac{1}{r_2} \approx \dfrac{1}{r}$	$V_i - V^* = -\dfrac{1}{b}(K_1 + K_2)\exp(-rt)$
	(ii) For $t \lesssim \dfrac{1}{r_1} \ll \dfrac{1}{r_2}$	$V_i - V^* = -\dfrac{1}{b}\{K_2\exp(-r_2t) + K_1(1 - r_1t)\}$
	(iii) For $t \lesssim \dfrac{1}{r_2} \ll \dfrac{1}{r_1}$	$V_i - V^* = -\dfrac{1}{b}\{K_2\exp(-r_2t) + K_1(1 - r_1t)\}$
	(iv) For $t \ll \dfrac{1}{r_1} \ll \dfrac{1}{r_2}$	$V^* - V_\infty = -IR_d + \dfrac{1}{b}(K_1r_1 + K_2r_2)t$
D	For $t \ll R_1C_1$	$V_i - V^* = -I\left(R_1 - \dfrac{t}{C_1}\right)$

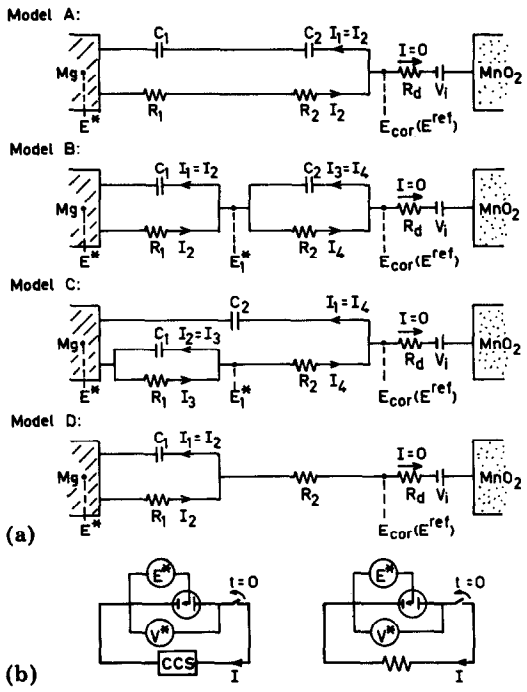

Fig. 12. (a) Electrical equivalent-circuit models A, B, C, and D representing Mg/MnO_2 dry cell following termination of discharge at constant current or across a constant resistance, R_L, without anode-film breakdown; (b) schematic electric circuit used in test. CCS: constant-current supply; R_L: constant-load resistance; E^*: single electrode potential of Mg anode during open-circuit recovery. Note: $I = 0$ and arrows indicate direction of conventional electric current.

data in order to test the theory and deduce the model that best describes the Mg/MnO_2 dry cell.

Steady-state results

According to Table 8, the steady-state cell voltage drop on discharge $(V_i - V_\infty)$ is linearly related to the discharge current $|I|$ for the four models and is governed by eqn. (10). Plots of $(V_i - V_\infty)$ *versus* $|I|$ obtained from experimental cell voltage transients (Figs. 3 and 4) are presented in Figs. 13 and 14. These plots are linear and, therefore, are in agreement with theory.

Values of the internal resistance $(R_1 + R_2 + R_d)$ can be obtained from the slopes of the plots in Figs. 13 and 14. These values are given in Table 10 and lie in the range 80 - 100 kΩ at 23 °C, and 500 - 800 kΩ at 0 °C. The large internal resistance observed during ultra-low rates of discharge demonstrates the absence of anode-film breakdown during the test.

TABLE 8

Diagnostic criteria from theoretical analysis of cell voltage transients of Mg/MnO_2 dry cell on initiating discharge at constant current without anode-film breakdown and comparison with experimental data

Criterion	Predicted result				Experimental results
	Model A	Model B	Model C	Model D	
$\ln(V - V_\infty)$ *vs.* t	linear	non-linear (Table 2) linear for cases (i) and (v) (Table 3)	non-linear (Table 2) linear for case (i) (Table 3)	linear	linear (Figs. 13, 14)
$(V_i - V)$ *vs.* t, as $t \to 0$	linear	linear	linear	linear	linear (Figs. 15, 16)
$V_i - V_{(t=0^+)}$	$-IR_d$	$-IR_d$	$-IR_d$	$-I(R_2 + R_d)$	very small 10 μV (Figs. 15, 16)
$(V_i - V_\infty)$ *vs.* $\lvert I \rvert$	linear	linear	linear	linear	linear (Figs. 11, 12)

TABLE 9

Diagnostic criteria from theoretical analysis of open-circuit cell voltage transients of Mg/MnO_2 dry cell on termination of constant-current discharge without anode-film breakdown and comparison with experimental data

Criterion	Predicted result				Experimental results
	Model A	Model B	Model C	Model D	
$\ln(V_i - V^*)$ *vs.* t	linear	non-linear (Table 5) linear for cases (i) and (v) (Table 7)	non-linear (Table 5) linear for case (i) (Table 7)	linear	linear (Fig. 17)
$(V^* - V)$ *vs.* t, as $t \to 0$	linear	linear	linear	linear	linear (Fig. 18)
$V - V^*_{(t=0^+)}$	IR_d	IR_d	IR_d	$I(R_2 + R_d)$	very small; 10 μV (Fig. 18)

Discharge transient

Plots of $\ln(V - V_\infty)$ *versus* t and $(V_i - V)$ *versus* t (as $t \to 0$), for the results of Figs. 3 and 4, are shown in Figs. 15 - 18. The plots are linear. The instantaneous cell voltage drop on initiation of discharge, *i.e.*, $(V_i - V_{(t=0^+)})$, is

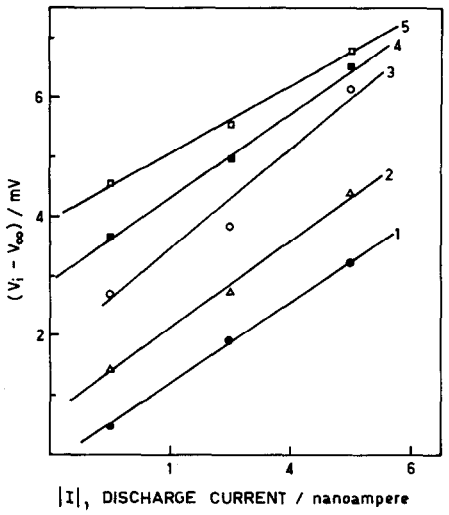

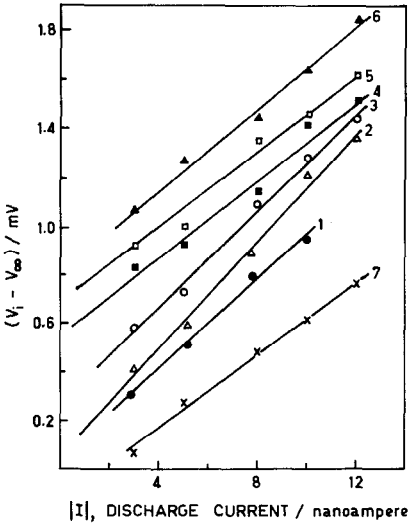

Fig. 13. Dependence of steady-state cell voltage drop, $(V_i - V_\infty)$, on discharge current during discharge of five Mg/MnO_2 cells at 0 °C without anode-film breakdown. For clarity, curves 2 - 5 have been shifted along ordinate by +1, +2, +3, +4 mV, respectively.

Fig. 14. Dependence of steady-state cell voltage drop $(V_i - V_\infty)$ on discharge current during the discharge of seven Mg/MnO_2 dry cells at 23 °C without anode-film breakdown. For clarity, curves 2 - 7 have been shifted along ordinate by +0.1, +0.3, +0.5, +0.7, +0.8, −0.2 mV, respectively.

seen to be less than 10 μV (*viz.*, the resolution limit of the measurement). From Table 8, it is seen that these experimental results are in agreement with the theoretical behaviour predicted by model A and certain special cases by that of model B and model C. Model D predicts an instantaneous cell voltage drop of $-I(R_2 + R_d)$. As will be seen below, $R_2 \approx (R_1 + R_2 + R_d)$ and, therefore, the predicted value of $(V_i - V_{t=0^+})$ is approximately equal to $(V_i - V_\infty)$. This is not observed experimentally and, consequently, model D is rejected.

Open-circuit recovery transient

Plots of $\ln(V_i - V^*)$ and $(V_\infty - V^*)$ *versus* t for the results of Figs. 3 and 4 are given in Figs. 19 and 20. The plots are linear. The instantaneous voltage jump on termination of discharge (Fig. 20) is less than 10 μV. From comparison with the criteria of Table 9, it can be seen that model A and certain special cases of model B and model C are applicable. Model D predicts an instantaneous voltage jump much larger than that observed experimentally and thus the model is inapplicable.

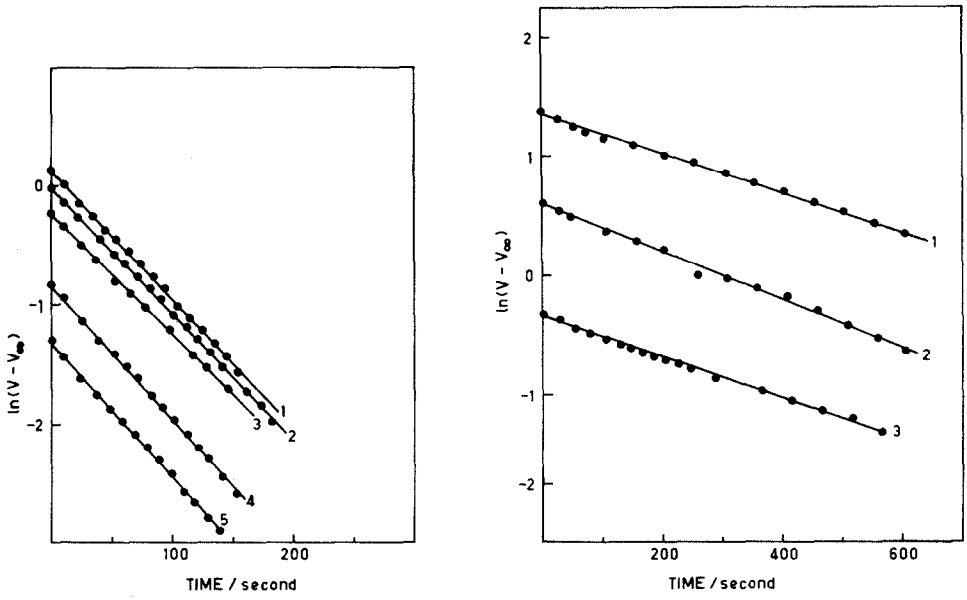

Fig. 15. Plot of $\ln(V - V_\infty)$ *vs.* time on initiating discharge at 23 °C for Mg/MnO_2 dry cell (*cf.*, Fig. 3); $(V - V_\infty)$ in mV. Discharge current (nA): (1) 12.0; (2) 10.0; (3) 8.0; (4) 5.0; (5) 3.0; Lines fitted by regression analysis, correlation coefficients: (1) 0.999; (2) 0.999; (3) 0.996; (4) 0.998; (5) 0.999.

Fig. 16. Plot of $\ln(V - V_\infty)$ *vs.* time on initiating discharge at 0 °C for Mg/MnO_2 dry cell (*cf.*, Fig. 4); $(V - V_\infty)$ in mV. Discharge current (nA): (1) 5.0; (2) 3.0; (3) 1.0. Lines fitted by regression analysis; all have a correlation coefficient of 0.999.

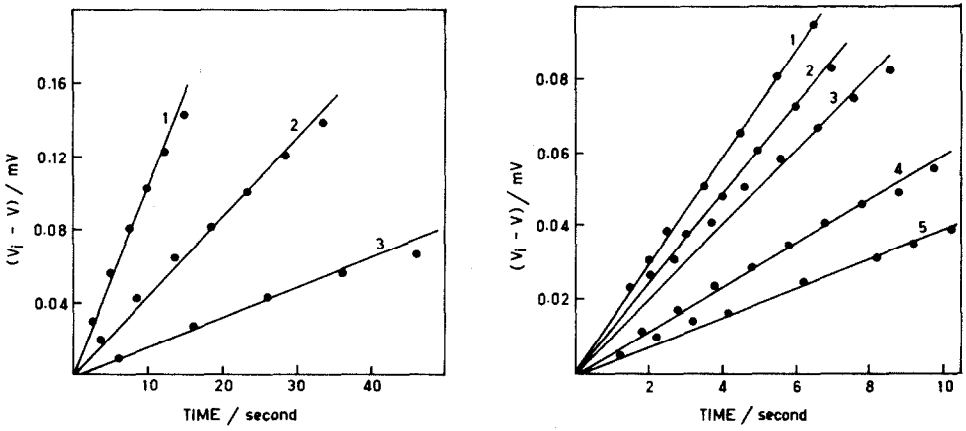

Fig. 17. Plot of $(V_i - V)$ *vs.* time on initiating discharge at 0 °C for Mg/MnO_2 dry cell (*cf.*, Fig. 4). Discharge current (nA): (1) 5.0; (2) 3.0; (3) 1.0. Lines fitted by regression analysis, correlation coefficients: (1) 0.997; (2) 0.998; (3) 0.997.

Fig. 18. Plot of $(V_i - V)$ *vs.* time on initiating discharge at 23 °C for Mg/MnO_2 dry cell (*cf.*, Fig. 3). Discharge current (nA): (1) 12.0; (2) 10.0; (3) 8.0; (4) 5.0; (5) 3.0. Lines fitted by regression analysis, correlation coefficients: (1) 0.999; (2) 0.999; (3) 0.996; (4) 0.998; (5) 0.998.

TABLE 10

Internal resistance of Mg/MnO_2 dry cells (CD-size) at 23 °C and 0 °C, with and without anode-film breakdown
Test current during discharge: (i) without anode-film breakdown, 10^{-8} - 10^{-9} A for 1 - 10 min; (ii) with anode-film breakdown, 10 mA for 10 min.

Cell no.	Internal resistance			
	23 °C		0 °C	
	without anode-film breakdown (kΩ)	with anode-film breakdown (Ω)	without anode-film breakdown (kΩ)	with anode-film breakdown (Ω)
1	97.9	2.0	629.6	4.2
2	106.6	1.6	654.6	4.0
3	82.6	1.5	690.2	3.8
4	97.1	1.6	804.9	3.8
5	83.5	1.5	543.4	3.8
6	80.9	1.7		
7	84.9	1.6		

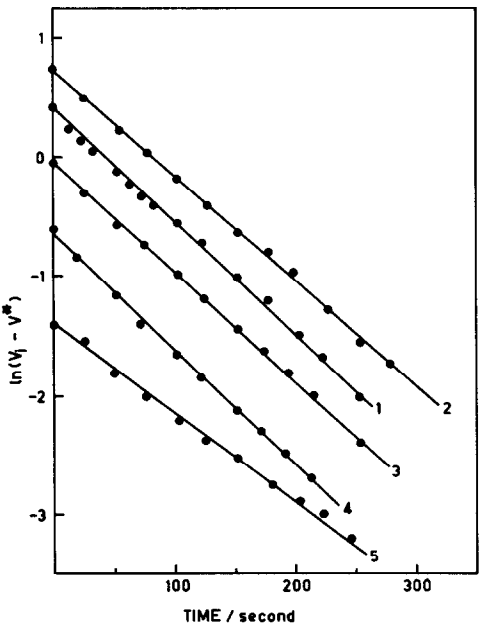

Fig. 19. Plot of $\ln(V_i - V^*)$ *vs.* time on termination of discharge of Mg/MnO_2 dry cell at 23 °C (*cf.*, Fig. 3). $(V_i - V^*)$ in mV. Discharge current (nA): (1) 12.1; (2) 10.0; (3) 8.0; (4) 5.0; (5) 3.0. For clarity, lines 2 and 5 have been shifted along ordinate by 0.50 and −0.50 units, respectively. Lines fitted by regression analysis, all have a correlation coefficient of 0.999.

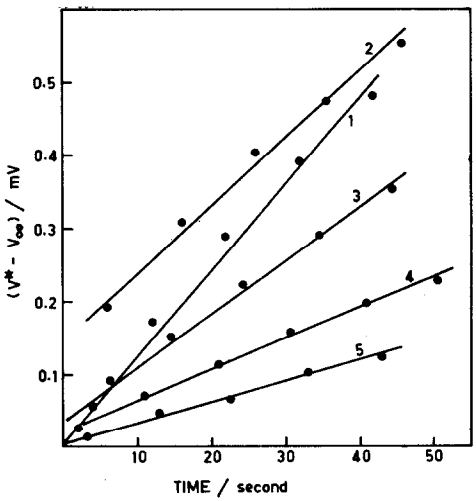

Fig. 20. Plot of $(V^* - V_\infty)$ *vs.* time on termination of discharge of Mg/MnO_2 dry cell at 23 °C (*cf.*, Fig. 3). Discharge current (nA): (1) 12.1; (2) 10.0; (3) 8.0; (4) 5.0; (5) 3.0. For clarity, line 2 has been shifted along ordinate by +0.1 mV.

Discussion

Evaluation of R_2

From the experimental results of Figs. 6 and 7, the value of 10^2 Ω to 0.5 Ω is found for the internal resistance of the Mg/MnO_2 dry cell during discharge (10^{-2} - 10^{-6} A for CD-size cell) accompanied by anode film breakdown. At discharge currents of 10^{-8} - 10^{-9} A the anode-film is intact and the internal resistance is 10^5 - 10^6 Ω (Table 10). This high value of internal resistance arises from the resistance of the passive film, R_2. Since the internal resistance of the cell after anode-film breakdown, *i.e.*, $R_1 + R_d$, is much smaller than that with the intact anode film, *i.e.*, $R_1 + R_2 + R_d$, the value of $(R_1 + R_2 + R_d)$ may be approximated to R_2 without significant error. Consequently, an accurate estimate of R_2 is obtained without the need to involve the transient response characteristics of the four models.

The high internal resistance for the cell (10^5 - 10^6 Ω for a CD-size cell), surprising as it may seem for a high energy primary cell, may be considered as an indication of good quality. This conclusion is only valid when the high value arises from resistance of the anode-film, and not from cell 'dry-out' or broken electrode connections.

Film resistance and delay time at 0 °C

From Table 10, it is seen that the value of $R_1 + R_2 + R_d$ at 0 °C is six times that at 23 °C. Since $(R_1 + R_2 + R_d)$ is governed by the magnitude of R_2, this finding suggests that the film resistance increases as the temperature is lowered. The negative temperature coefficient is consistent with the behaviour of insulator materials at ambient or moderately elevated temperatures due to the presence of defects [10]. In general, an increase in film resistance is expected to make breakdown of the anode film more difficult during discharge [3, 4]; a situation that is characterized by an enhanced 'delay time' during cell operation (Table 1). Note, 'delay time' is defined as the time that elapses following initiation of discharge before a specified operating voltage is attained. Thus, the determination of anode film resistance may be exploited in the optimisation of passivation coatings for improved performance with reduced delay time.

Equivalent circuit model

Comparison of experimental results with theory shows that model D (Fig. 10(a)) is inapplicable. On the other hand, model A and special cases of model B (cases (i) and (v), Table 3) and model C (case (i), Table 3) are found to be in agreement with theory. A distinction between the relative plausibility of the latter three cases and evaluation of all the system parameters is not possible at the present stage. Information from a.c. impedance measurements can be used to achieve this distinction [11].

Conclusions

The above experimental and theoretical investigations of voltage transients of Mg/MnO_2 dry cells demonstrate the methodology of a

non-destructive electrochemical technique for the study of the passive film-covered anode/solution interface in high-energy primary batteries. Several improvements in experimental technique over previous attempts have been effected. The analysis considers, comprehensively, several possible equivalent circuit models for the anode/solution interface and leads to the choice of a set of plausible descriptions.

The resistance of the passive film on the anode and the dependence of its value on temperature may be used to achieve quality control and design optimisation of Mg/MnO_2 cells. This technique can, in principle, be extended to other battery systems based on lithium, aluminium, calcium, etc.

List of symbols

R_1	Charge-transfer resistance for anodic ionisation of magnesium (in the equivalent circuit)
R_2	Resistance of dielectric film on anode (in the equivalent circuit)
R_d	Resistance of electrolyte, cathode mix, and separator
R	$R_1 + R_2 + R_d + R_L$; also gas constant
R_L	Constant load resistance
C_1	Double layer capacitance at anode–film interface
C_2	Capacitance of dielectric film on anode
V	Cell voltage during constant current discharge
V_i	Open-circuit voltage of the magnesium–manganese dioxide cell prior to discharge
V^*	Open-circuit cell voltage following termination of discharge at any time t
$V_{t=0^+}$	Cell voltage immediately on initiating discharge
V_∞	Cell voltage in the steady state at given I
$V^*_{t=0^+}$	Open-circuit cell voltage immediately on terminating discharge
E_c	Single electrode potential of the cathode (MnO_2 electrode)
E_a	Single electrode potential of the anode (Mg electrode)
E_{cor}	Steady-state corrosion potential of the magnesium anode
E	Single electrode potential of the magnesium anode during discharge at any time t
E^*	Open-circuit single electrode potential of magnesium anode following termination of discharge at any time t
I	Discharge current
α, β	Transfer coefficients

References

1 A. N. Dey, *Thin Solid Films, 43* (1977) 131.
2 B. V. Ratnakumar and S. Sathyanarayana, *J. Power Sources, 10* (1983) 219.

3 C. R. Schlaigker, in J. P. Gabano (ed.), *Lithium Batteries*, Academic Press, London, 1983.
4 S. Sathyanarayana and B. V. Ratnakumar, *J. Power Sources, 10* (1983) 243.
5 S. R. Narayanan and S. Sathyanarayana, *J. Power Sources, 15* (1985) 27.
6 R. V. Moshtev and Y. Geronov, *J. Power Sources, 8* (1982) 395.
7 R. V. Moshtev, Y. Geronov and B. Purusheva, *J. Electrochem. Soc., 128* (1981) 1851.
8 S. R. Narayanan and S. Sathyanarayana, *J. Power Sources, 24* (1988) 51.
9 E. Peled, in J. P. Gabano (ed.), *Lithium Batteries*, Academic Press, London, 1983.
10 W. C. Mackrodt and R. F. Stewart, *J. Phys. C: Solid State Phys., 10* (1977) 1431.
11 S. R. Narayanan and S. Sathyanarayana, unpublished work.

Appendix 1

Cell voltage transient analysis on initiating a constant current discharge for model C (Fig. 10(a))

The equivalent circuit, model C, during discharge of an Mg/MnO_2 dry cell sustaining a constant current I without any anode-film breakdown is shown in Fig. 10(a).

The discharge current I is related to the branch currents as follows:

$$I = I_1 + I_4 = I_1 + I_2 + I_3 \tag{A1}$$

The potential E_1 of the equi-potential surface between R_2 and the parallel combination of R_1 and C_1 is related to the branch currents as follows:

$$I_1 = -C_2 \frac{\mathrm{d}(E - E_{cor})}{\mathrm{d}t} \tag{A2}$$

$$I_2 = -C_1 \frac{\mathrm{d}(E - E_1)}{\mathrm{d}t} \tag{A3}$$

$$I_3 = -\frac{E - E_1}{R_1} \tag{A4}$$

$$I_4 = -\frac{E_1 - E_{cor}}{R_2} \tag{A5}$$

From eqns. (A1) - (A3):

$$I = -C_2 \frac{\mathrm{d}(E - E_{cor})}{\mathrm{d}t} - C_1 \frac{\mathrm{d}(E - E_1)}{\mathrm{d}t} - \frac{E - E_1}{R_1} \tag{A6}$$

From eqns. (A1), (A2) and (A5):

$$-\frac{E_1 - E_{cor}}{R_2} = I + C_2 \frac{\mathrm{d}(E - E_{cor})}{\mathrm{d}t} \tag{A7}$$

or

$$E_1 - E_{cor} = -IR_2 - R_2C_2 \frac{d(E - E_{cor})}{dt} \quad \text{(A8)}$$

Equation (A7) may be written as:

$$\frac{E - E_1}{R_2} - \frac{E - E_{cor}}{R_2} = I + C_2 \frac{d(E - E_{cor})}{dt} \quad \text{(A9)}$$

Solving for $E - E_1$:

$$E - E_1 = IR_2 + E - E_{cor} + R_2C_2 \frac{d(E - E_{cor})}{dt} \quad \text{(A10)}$$

Differentiating eqn. (A9) with respect to t:

$$\frac{d(E - E_1)}{dt} = \frac{d(E - E_{cor})}{dt} + R_2C_2 \frac{d^2(E - E_{cor})}{dt^2} \quad \text{(A11)}$$

From eqns. (A6), (A10) and (A11):

$$\frac{d^2(E - E_{cor})}{dt^2} + \frac{R_1C_1 + R_2C_2 + R_1C_2}{R_1C_1R_2C_2} \frac{d(E - E_{cor})}{dt} + \frac{E - E_{cor}}{R_1C_1R_2C_2} = -\frac{I(R_1 + R_2)}{R_1C_1R_2C_2} \quad \text{(A12)}$$

Substituting $E - E_{cor}$ from eqn. (3) in eqn. (A12):

$$\frac{d^2V}{dt^2} + \frac{R_1C_1 + R_2C_2 + R_1C_2}{R_1C_1R_2C_2} \frac{dV}{dt} + \frac{V}{R_1C_1R_2C_2} = \frac{V_i + I(R_1 + R_2 + R_d)}{R_1C_1R_2C_2} \quad \text{(A13)}$$

The solution of eqn. (A13) is:

$$V_i - V = -I(R_1 + R_2 + R_d) - \frac{1}{b}\{K_1 \exp(-r_1 t) + K_2 \exp(-r_2 t)\} \quad \text{(A14)}$$

where

$$a = \frac{R_1C_1 + R_2C_2 + R_1C_2}{R_1C_1R_2C_2}$$

$$b = \frac{1}{R_1C_1R_2C_2}$$

r_1 and r_2 are the roots of the characteristic equation for the differential equation (A14) and are given by

$$r_1 = \frac{a + (a^2 - 4b)^{1/2}}{2}$$

$$r_2 = \frac{a - (a^2 - 4b)^{1/2}}{2}$$

K_1 and K_2 are integration constants.

It follows from Fig. 8(a) for model C that at $t = 0^+$, the instantaneous current is shunted by C_1 and C_2, and this leads to an instantaneous cell voltage:

$$V_{(t=0^+)} = V_i + IR_d \tag{A15}$$

Hence, from eqns. (A14) and (A15):

$$K_1 + K_2 = -\frac{I(R_1 + R_2)}{R_1C_1R_2C_2} \tag{A16}$$

However, unless another boundary condition is available, K_1 and K_2 cannot be separately evaluated.

Appendix 2

Cell voltage transient analysis on initiating discharge across a constant resistance for model C (Fig. 11(a))

The equivalent circuit, model C, for the Mg/MnO_2 dry cell during discharge across a constant resistance without anode-film breakdown is shown in Fig. 11(a).

From eqns. (A2) - (A4):

$$I = -C_2\frac{d(E - E_{cor})}{dt} - C_1\frac{d(E - E_1)}{dt} - \frac{E - E_1}{R_1} \tag{A17}$$

From eqn. (A10):

$$E - E_1 = IR_2 + E - E_{cor} + R_2C_2\frac{d(E - E_{cor})}{dt} \tag{A18}$$

Differentiating eqn. (A18) with respect to t:

$$\frac{d(E - E_1)}{dt} = R_2\frac{dI}{dt} + \frac{d(E - E_{cor})}{dt} + R_2C_2\frac{d^2(E - E_{cor})}{dt^2} \tag{A19}$$

From eqns. (A17) - (A19):

$$\frac{d^2(E - E_{cor})}{dt^2} + \frac{1}{R_1C_1} + \frac{1}{R_2C_2} + \frac{1}{R_2C_1}\frac{d(E - E_{cor})}{dt} + \frac{E - E_{cor}}{R_1C_1R_2C_2} = -\frac{I(R_1 + R_2)}{R_1C_1R_2C_2} - \frac{1}{C_2}\frac{dI}{dt} \tag{A20}$$

Substituting for I and $(E - E_{cor})$ from eqns. (5) and (7):

$$\frac{d^2V}{dt^2} + a\frac{dV}{dt} + bV + c = 0 \tag{A21}$$

where:

$$a = \frac{1}{R_1C_1} + \frac{1}{R_2C_2} + \frac{1}{R_2C_1} + \frac{1}{(R_L + R_d)C_2}$$

$$b = \frac{R_1 + R_2 + R_L + R_d}{R_1C_1R_2C_2(R_L + R_d)}$$

$$c = \frac{V_iR_L}{R_1C_1R_2C_2(R_L + R_d)}$$

The solution to eqn. (A21) is of the same form as eqn. (A14), *viz.*,

$$V = \frac{1}{b}\{K_1 \exp(-r_1t) + K_2 \exp(-r_2t) - c\} \quad \text{(A22)}$$

r_1 and r_2 are the roots of the characteristic equation for eqn. (A21) and are given by

$$r_1 = \frac{a - (a^2 - 4b)^{1/2}}{2}$$

$$r_2 = \frac{a + (a^2 - 4b)^{1/2}}{2}$$

K_1 and K_2 are integration constants.

At $t = 0^+$ (*i.e.*, immediately after initiation of discharge), the cell voltage is given by:

$$V_{(t=0^+)} = \frac{V_iR_L}{R_L + R_d} \quad \text{(A23)}$$

R_1 and R_2 are shunted by C_1 and C_2 for any instantaneous current and thus do not appear in eqn. (A23).

Hence:

$$K_1 + K_2 = \frac{bV_iR_L}{R_L + R_d} + c \quad \text{(A24)}$$

However, no additional boundary condition is available to evaluate K_1 and K_2 separately.

Appendix 3

Analysis of open-circuit cell voltage recovery transient on termination of discharge for model C (Fig. 12(a))

Case (i): Open-circuit voltage recovery transient of Mg/MnO_2 dry cell following termination of constant-current discharge without anode-film breakdown

The governing differential equation for the open-circuit recovery transient following the termination of constant-current discharge for model

C (Fig. 10(a)) can be obtained by setting $I = 0$ in eqn. (A2) and replacing V by V^* to denote the open-circuit condition, *i.e.*,

$$\frac{d^2V^*}{dt^2} + a\frac{dV^*}{dt} + bV^* + c = 0 \tag{A25}$$

where:

$$a = \frac{1}{R_1C_1} + \frac{1}{R_2C_2} + \frac{1}{R_2C_1}$$

$$b = \frac{1}{R_1C_1R_2C_2}$$

$$c = \frac{V_i}{R_1C_1R_2C_2}$$

The solution of eqn. (A25) is:

$$V^* = \frac{1}{b}\{K_1 \exp(-r_1t) + K_2 \exp(-r_2t) - c\} \tag{A26}$$

r_1 and r_2 are positive real roots of the characteristic equation for eqn. (A25) and

$$r_1 = \frac{a - (a^2 - 4b)^{1/2}}{2}$$

$$r_2 = \frac{a + (a^2 - 4b)^{1/2}}{2}$$

K_1 and K_2 are integration constants.

At $t = 0^+$ (*i.e.*, immediately after termination of discharge) the cell voltage is given by (Figs. 10(a) and 12(a)):

$$V^*_{(t=0^+)} = V_\infty - IR_d$$

$$= V_i + I(R_1 + R_2) \tag{A27}$$

From eqns. (A26) and (A27):

$$K_1 + K_2 = \frac{I(R_1 + R_2)}{R_1C_1R_2C_2}$$

However, unless another boundary condition is available, K_1 and K_2 cannot be evaluated.

Case (ii): Open-circuit voltage recovery transient of Mg/MnO_2 dry cell following termination of discharge across a constant resistance without anode film breakdown

The equation describing the open-circuit cell voltage recovery transient following termination of constant resistance discharge is identical to eqn. (A26), *viz.*,

$$V^* = \frac{1}{b}\{K_1 \exp(-r_1 t) + K_2 \exp(-r_2 t) - c\} \tag{A28}$$

Since the cell voltage immediately on termination of discharge is obtained analogous to eqn. (A27) as

$$V_{(t=0^+)} = \frac{V_i(R_L + R_d)}{R_1 + R_2 + R_L + R_d} \tag{A29}$$

$$K_1 + K_2 = \frac{bV_i(R_L + R_d)}{R_1 + R_2 + R_L + R_d} + c \tag{A30}$$

As before, K_1 and K_2 cannot be separately evaluated without an additional boundary condition.